X-ray and Optical Spectral Properties of Active Galactic Nuclei

by

Laura Elizabeth Trouille

A dissertation submitted in partial fulfillment of the requirements for the degree of

Doctor of Philosophy
(Astronomy)

at the

University of Wisconsin – Madison

2010

Il est encore plus facile de juger
de l'esprit d'un homme
par ses questions que par ses réponses.

- Voltaire

Acknowledgements

First, I thank my advisor Amy Barger for providing me the resources, guidance, and independence to make this thesis my own. Above all, I am grateful to Amy for helping me understand which questions are worthwhile to pursue in this vast and beautiful subject of ours.

I am thankful for conversations with Christy Tremonti, Sebastian Heinz, Jay Gallagher, and John Everett, which were helpful not just for their scientific content, but for keeping me excited about my own science as well. I would like to acknowledge Ed Churchwell and Matt Haffner, excellent astronomers and genuinely good people, for their kind words of encouragement. I am grateful for the influence of Brian Chaboyer, my undergraduate mentor at Dartmouth, who helped me feel confident of my ability as a researcher.

This thesis would not have been possible without the expertise of Stephan Jansen, our system administrator. I am so grateful for his quick diagnoses and readiness to help. And a big thank you to Steve Anderson, John Varda, and Lynn Thiele for keeping our department running smoothly with a smile.

Thank you to the National Science Foundation for the graduate research fellowship which allowed me the flexibility to pursue my two passions in astronomy– research and education/outreach. I would like to thank Eric Wilcots for the 'Universe in the Park' program and Jim Lattis, Kay Kriewald, and Janet Niewold for making Space Place a wonderful venue for science enrichment in our community. Sharing my love of astronomy with the public has fueled my momentum through these graduate school years.

While trying to organize anything among astronomers is like herding cats, it has been an honor and a pleasure to be a part of this young community. Thank you to Emily and Laura for founding WOWSA with me and to Natalie, Katelyn, and Blakesley for taking up the torch. As one-by-one Kyle, Tommy, Emily, Devine, Chomiuk, Matt, and more have flown the coop, I've realized how lucky I am to have overlapped with such kind, unique individuals.

I owe my deepest gratitude to my parents who value education and have given me the confidence to pursue my dreams, whatever they may be. They have shared with me their curiosity of the world around them, its cultures and people, and have taught me by example to think deeply and cherish my individuality.

Last, but not least, it is a pleasure to thank my hubby-to-be for being a calm, loving, and insightful friend. Who would have guessed years ago when you walked into our first-year office that this is what the future held? I look forward to the happiness of our years together, under the twinkling sky.

Contents

Acknowledgements ii

List of Tables vii

List of Figures ix

1 Introduction **1**

1.1 Motivation 2

1.2 X-ray versus Optical Spectral Properties of AGNs 2

1.3 Is [OIII] a Reliable Indicator of AGN Activity? 6

1.4 The Elusive Population of Compton-thick AGNs 7

1.5 The OPTX Survey Fields 10

1.5.1 CDF-N 10

1.5.2 CLASXS & CLANS 10

1.6 Thesis Goals and Outline 10

References 11

2 The OPTX Project I: The Flux and Redshift Catalogs for the CLANS, CLASXS, and CDF-N Fields **16**

Abstract 17

2.1 Introduction 18

2.2 X-ray Properties 20

2.2.1 CLANS X-ray Observations 20

2.2.2 CLANS X-ray Source Detection and Fluxes 21

2.2.3 CLANS X-ray Catalog 23

2.2.4 Flux Limits 23

2.2.5 Effective Areas . . . 24
2.3 Optical and IR Imaging . . . 27
2.3.1 MegaCam . . . 27
2.3.2 WIRCam . . . 28
2.3.3 ULBCam . . . 29
2.3.4 WFCAM . . . 29
2.3.5 Spitzer . . . 30
2.3.6 Optical and NIR Source Detection and Photometry . . . 30
2.3.7 CLASXS: Updated Optical Photometry . . . 32
2.4 Redshift Information . . . 32
2.4.1 Spectroscopic Observations . . . 32
2.4.2 Spectroscopic Completeness . . . 34
2.4.3 Photometric Redshifts . . . 34
2.4.4 Redshift and Flux Distributions . . . 37
2.5 Optical Spectral Classification . . . 42
2.6 Optical/IR Counterparts Catalogs . . . 44
2.6.1 CLANS . . . 44
2.6.2 CLASXS . . . 44
2.6.3 CDF-N . . . 45
2.7 X-ray Luminosities . . . 45
2.8 Number Counts . . . 47
2.9 Summary . . . 52
References . . . 52

3 The OPTX Project III: X-ray Versus Optical Spectral Type for AGNs 56
Abstract . . . 57
3.1 Introduction . . . 58
3.2 X-ray Data . . . 60
3.3 Classification by Optical Spectral Type . . . 61
3.4 Comparison of Optical Classification with X-ray Classification . . . 64

3.4.1 $\Gamma_{\rm eff}$ Distributions . . . 64
3.4.2 $\Gamma_{\rm eff}$ versus X-ray Luminosity . . . 69
3.5 Discussion . . . 72
3.6 Conclusions . . . 74
References . . . 74

4 The OPTX Project IV: How Reliable is [OIII] as a Measure of AGN Activity? 78
Abstract . . . 79
4.1 Introduction . . . 80
4.2 Sample . . . 81
4.3 High-Ionization Narrow Emission Lines . . . 82
4.3.1 [OIII]λ5007 . . . 82
4.3.2 Emission-Line Reddening . . . 84
4.4 Emission-Line Ratio Diagnostic Diagrams . . . 86
4.5 The Relation Between $L_{\rm [OIII]}$ and L_X . . . 87
4.6 Discussion . . . 92
4.7 Summary . . . 96
References . . . 98

5 The OPTX Project V: Identifying Distant Compton-thick AGNs 101
Abstract . . . 102
5.1 Introduction . . . 103
5.2 Sample . . . 104
5.2.1 SDSS . . . 104
5.2.2 OPTX . . . 105
5.2.3 GOODS-N . . . 106
5.2.4 Rest-frame $g-z$ Color . . . 106
5.3 High-Redshift Optical Emission Line Diagnostic . . . 106
5.4 Identifying X-ray Selected AGNs Using Optical Emission Line Diagnostics . . . 109
5.5 Identifying X-ray Faint/Undetected AGNs using Optical Emission Line Diagnostics . . . 109

5.6 Application: Identifying Compton-thick AGNs 110
5.7 Discussion 114
5.7.1 A New Diagnostic Diagram for Galaxies at Redshifts up to 1.4 114
5.7.2 CT AGN Space Densities compared with X-ray Background Models 116
5.8 Summary 117
References 119

6 Conclusions **122**

6.1 Thesis Results 123
6.2 Completion of OPTX Project V 126
References 129

List of Tables

2.1 Spectroscopic Completeness of Selected Surveys from the Literature 19
2.2 CLANS Observation Summary 20
2.3 X-ray Data Specifications 21
2.4 CLANS X-ray Catalog: Basic Source Properties 23
2.5 CLANS X-ray Catalog: Additional Source Properties 24
2.6 CLANS Optical & Near-IR Specifications 31
2.7 CLASXS Optical & Near-IR Specifications 32
2.8 CDF-N Near-IR Specifications 33
2.9 CLASXS Zeropoint Offsets 34
2.10 X-ray Samples by Field and Optical Spectral Class 42
2.11 CLANS Optical/IR Counterparts Catalog 43
2.12 CLASXS Optical/IR Counterparts Catalog 43
2.13 CDF-N Optical/IR Counterparts Catalog 44
2.14 Best-fit to the Number Counts 47

3.1 CLANS, CLASXS, and CDF-N Survey Characteristics 61
3.2 CLANS Catalog, Updated Sources 62
3.3 Optical Spectral Classification for our $2-8$ keV Sample 63
3.4 Non-BLAGNs with Soft Photon Indices 71

4.1 $\log(L_{[\mathrm{OIII}]}/L_X)$ 89
4.2 Best fits to the luminosity dependent ratio of $L_{[\mathrm{OIII}]}/L_X$ 91

5.1 GOODS-N $z < 0.5$ Candidate AGNs 110

5.2 GOODS-N $z < 1.4$ Candidate AGNs 113

5.3 CT AGN Space Density Determinations from the Literature 118

List of Figures

1.1 Composite Spectra of Broad-Line and non-Broad-Line AGNs 3
1.2 Simple Unified Model for AGNs 4
1.3 Redshift Bias in X-ray Classification 5
1.4 Clumpy Torus and Disk-Wind Models for AGN Obscuration 6
1.5 Observed Extragalactic X-ray Background 8

2.1 Location of the CLANS and CLASXS pointings 22
2.2 Flux vs. Off-axis Angle for the OPTX Sources 25
2.3 Probability of Source Detection 27
2.4 Fraction of Annulus within ACIS-I Chip 28
2.5 Total Effective Area 29
2.6 Spectroscopic Completeness 35
2.7 Template SEDs 37
2.8 Reliability of Photo-z Determinations 38
2.9 Comparison of Template Fitting and HYPERZ Methods 39
2.10 OPTX Redshift Distribution 39
2.11 OPTX $0.5-2$ keV Flux Distribution 40
2.12 OPTX $2-8$ keV Flux Distribution 41
2.13 X-ray Luminosity vs. Redshift 46
2.14 Differential Number Counts 49
2.15 Differential Number Counts, Residuals 50
2.16 Comparison of Number Counts Fits from Other Surveys 51

3.1 $2-8$ keV Flux Distribution . . . 62
3.2 R Magnitude vs. $2-8$ keV Flux . . . 64
3.3 Spectroscopic Completeness . . . 65
3.4 Redshift Distribution by Optical Spectral Type . . . 66
3.5 $\Gamma_{\rm eff}$ Distribution by Optical Spectral Type . . . 67
3.6 $I-J$ vs. $J-K$ for our X-ray Hard BLAGNs . . . 68
3.7 $\Gamma_{\rm eff}$ vs. X-ray Luminosity . . . 70
3.8 $\Gamma_{\rm eff}$ vs. X-ray Luminosity in Redshift Bins . . . 72

4.1 L_X vs. Redshift for our $2-8$ keV Sample . . . 83
4.2 Emission-line Reddening Correction . . . 84
4.3 BPT Diagram Applied to our $2-8$ keV Sample . . . 87
4.4 Distribution of $L_{\rm [OIII]}/L_X$ for our $2-8$ keV Sample . . . 88
4.5 $L_{\rm [OIII]}/L_X$ vs. L_X for our OPTX Non-BLAGNs . . . 90
4.6 $L_{\rm [OIII]}/L_X$ vs. L_X for our OPTX BLAGNs . . . 91
4.7 BPT Diagram, Increasing $L_{\rm [OIII]}/L_X$ . . . 93
4.8 $L_{\rm [OIII]}/L_X$, Sources with Reliable Balmer Fluxes . . . 94
4.9 $L_{\rm [OIII]}/L_X$ vs. L_X, BLAGN Comparison . . . 95
4.10 Comparison of X-ray and OIII LFs . . . 97

5.1 BPT Diagram Applied to the SDSS DR7 Galaxies . . . 107
5.2 High-redshift Diagnostic Applied to the SDSS DR7 Galaxies . . . 108
5.3 High-redshift Diagnostic Applied to our OPTX Non-BLAGNs . . . 109
5.4 BPT Diagram Applied to the GOODS-N Galaxies . . . 111
5.5 High-redshift Diagnostic Applied to the GOODS-N Galaxies . . . 112
5.6 Distribution in $L_{\rm [NeIII]}/L_X$ for our OPTX Non-BLAGNs . . . 113
5.7 Location of LINERs in the BPT Diagram . . . 114
5.8 Comparison of CT AGN Space Densities from the Literature . . . 117

6.1 BPT Diagram for the CLANS Galaxy Survey . . . 128

Chapter 1

Introduction

1.1 Motivation

Active Galactic Nuclei (AGNs) are cosmological powerhouses that emit prodigious amounts of light over several decades in energy. They number among the most luminous radio, optical, and X-ray sources known. This relatively uniform, luminous, multi-band emission from AGNs is non-stellar in origin. AGN unification models suggest that all AGNs are powered by accretion onto a supermassive black hole (SMBH; $M_{BH} \geq 10^6\ M_{\odot}$) that resides at the center of the galaxy (see Antonucci 1993 for a review).

Current observations suggest that most galaxies, including the Milky Way, have a SMBH at their centers (Kormendy & Richstone 1995; Magorrian et al. 1998; van der Marel 1999). Moreover, the mass of the SMBH appears to be tied to the mass of the host galaxy's bulge from studies of both velocity dispersion (Ferrarese & Merritt 2000; Gebhardt et al. 2000) and the bulge luminosity (Magorrian et al. 1998). This strongly suggests that the formation of the host galaxy and its SMBH are somehow connected.

Hard $2-8$ keV X-ray surveys provide as complete and unbiased a sample of AGNs as is presently possible (Mushotzky et al. 2004). At these energies, dilution of the AGN light by the stellar light from the host galaxy is minimal, and the cross-section of the circumnuclear obscuring material drops quickly with increasing X-ray energy, enabling hard X-ray photons to penetrate all but the densest material. X-ray surveys have so far found the highest density of AGNs on the sky (≥ 5500 deg^{-2}, as compared to ~ 400 deg^{-2} for the deepest optical surveys). Ultradeep *Chandra* X-ray surveys (Mushotzky et al. 2000; Brandt et al. 2001; Giacconi et al. 2002; Alexander et al. 2003; Barger et al. 2005; Luo et al. 2008) have resolved nearly 100% of the $2-8$ keV X-ray background (XRB; see Churazov et al. 2007 for a recent measurement of the XRB using INTEGRAL and Gilli et al. 2007 and Frontera et al. 2007 for in-depth comparisons of the various XRB measurements to date). Even though the majority of the $0.5-8$ keV XRB has been resolved into discrete sources, the nature of the sources is still unfolding.

The increased emergence of wide-field, multi-object spectrographs like HYDRA (Barden et al. 1994) on the WIYN 3.5 m telescope and the DEep Imaging Multi-Object Spectrograph (DEIMOS; Faber et al. (2003) on the Keck 10 m telescope on Mauna Kea greatly improves the efficiency of spectroscopic surveys designed to examine the optical properties and measure redshifts for these X-ray detected AGNs. The combination of X-ray and optical data allows one to study the X-ray/optical AGN connection and its evolution over cosmic time.

1.2 X-ray versus Optical Spectral Properties of AGNs

There are striking differences in the optical spectra of AGNs. Some show broad (FWHM > 2000 km s^{-1}) emission lines while others exhibit narrow (FWHM ~ 400 km s^{-1}) forbidden emission lines (see Figure 1.1). One generally assumes that there is less intrinsic diversity among AGNs than we observe, and that the variety of AGN phenomena is due to a combination of real differences in a small number of physical parameters (like luminosity) coupled with apparent differences which are due to observer-dependent parameters (like orientation). In the Antonucci (1993) simple unified model for AGNs, it is the geometry of a dust torus which determines the amount of obscuring material along the observer's line of sight to the central X-ray emitting regions, as well as which region (broad-line or narrow-line) one is observing. In this

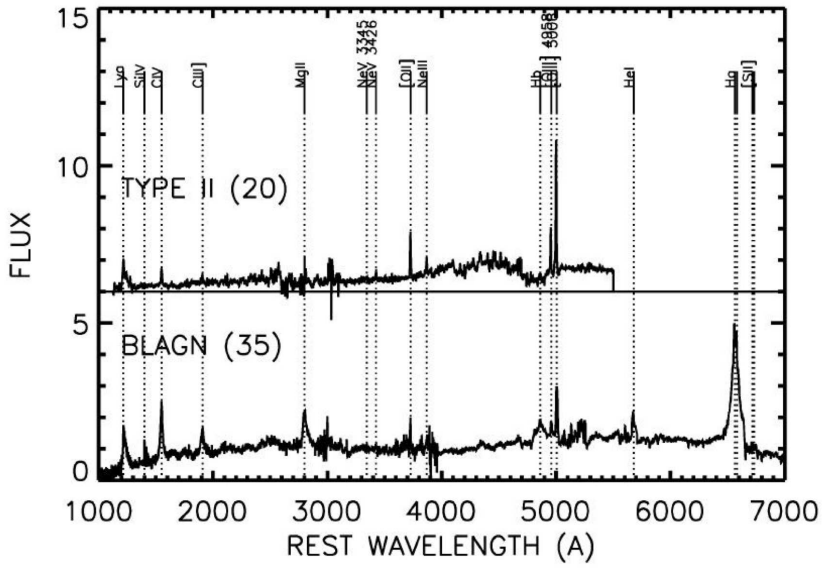

Fig. 1.1. — Composite spectra of 35 broad-line AGNs and 20 non-broad-line AGNs, reproduced from Barger et al. (2005).

model, broad-line AGNs are unobscured sources in which one is seeing down the ionization cone to clouds in high density regions within ~ 0.003 parsecs of the accretion disk. Non-broad-line AGNs, on the other hand, are observed when the central source is obscured by the circumnuclear material and the emission lines come from lower density clouds at $30 - 100$ parsecs from the accretion disk (see Figure 1.2 showing the Urry & Padovani 1995 cartoon depiction of the simple unified model for AGNs).

X-ray data alone have also long been used to estimate the amount of obscuration between the observer and the nuclear source through the $0.5-8$ keV spectral slope. Since $2-8$ keV X-rays will penetrate obscuring material (except in Compton-thick AGNs, where the neutral hydrogen column density, N_H, in the line of sight is higher than the inverse Thomson cross section, $N_H = 1.5 \times 10^{24}$ cm^{-2}) and $0.5 - 2$ keV X-rays will not, in low signal-to-noise data a shallower slope may indicate an obscured source. X-ray spectra can be approximated with a power-law of the form $P(E) = AE^{-\Gamma_{\rm eff}}$, where E is the photon energy in keV and A is the normalization factor. (Here, we indicate the power-law slope as $\Gamma_{\rm eff}$ to distinguish it from the intrinsic slope, Γ. $\Gamma_{\rm eff}$ is not the true Γ unless there is no intrinsic absorption.)

Hasinger et al. (2005) initiated a current trend in the field to combine the X-ray and optical classification schemes in order to create the most 'complete' sample of unobscured AGNs. Unobscured AGNs, in this scenario, include any object optically classified as a broad-line AGN, as well as any object satisfying $L_X \geq 10^{42}$ erg s^{-1} and $\Gamma_{\rm eff} \geq 1.2$. This decision was based on their assumption that 'true' broad-line

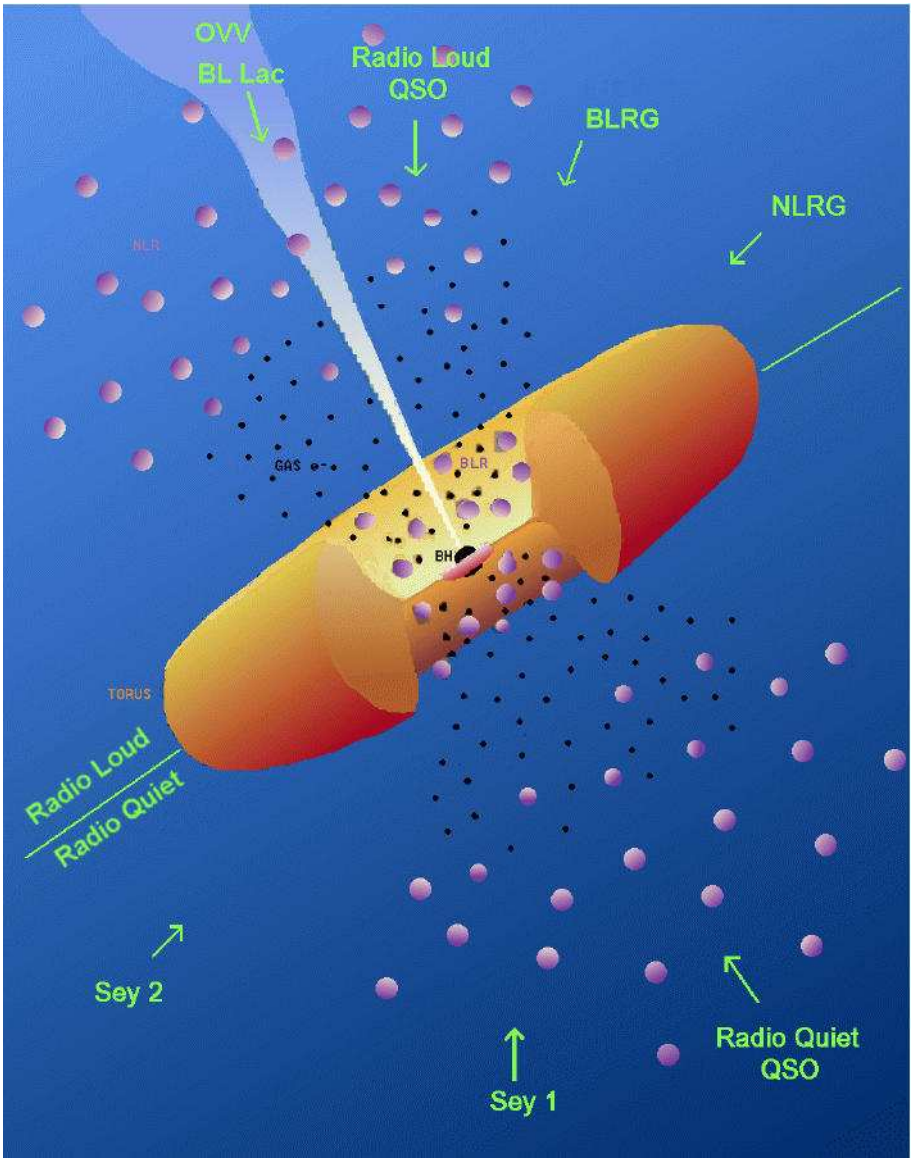

Fig. 1.2. — Cartoon depiction of the simple unified model for AGNs, reproduced from Urry & Padovani (1995).

AGNs may be optically misclassified as non-broad-line AGNs due to dilution of the AGN light by the host galaxy light, particularly at low luminosities (Moran et al. 2002; Severgnini et al. 2003; Garcet et al. 2007; Cardamone et al. 2007).

The creation of a classification scheme that mixes optical and X-ray spectral diagnostics requires a thorough understanding of the correspondence between X-ray and optical spectral type. Unfortunately, $10-30\%$ of AGNs have (1) X-ray spectra that show no absorption and (2) optical spectra that suggest obscuration (e.g., Pappa et al. 2001; Panessa & Bassani 2002; Barcons et al. 2003; Georgantopoulos & Zezas 2003; Caccianaga et al. 2004; Corral et al. 2005; Wolter et al. 2005; Tozzi et al. 2006). The opposite effect, i.e., (1) X-ray spectra that show absorption and (2) optical spectra that suggest no obscuration, has also

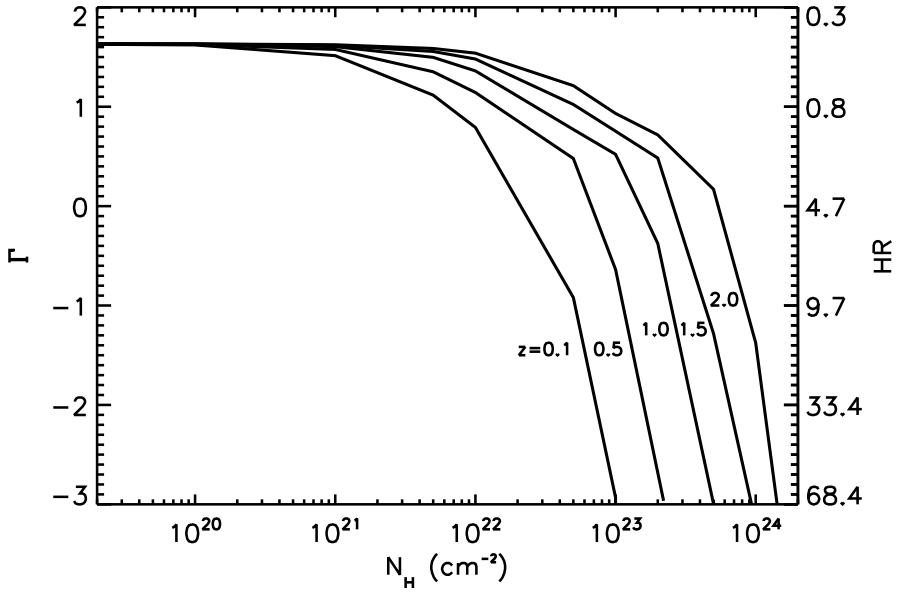

Fig. 1.3. — Γ_{eff} vs. N_H for $z = 0.1$, 0.5, 1.0, 1.5, and 2.0, as labeled. The right-hand y-axis provides the corresponding values for the *Chandra*-specific hardness ratio ($2-8$ keV count rate divided by the $0.5-2$ keV count rate). Values determined using WEBPIMMS, assuming a spectral index of 1.7 and the Galactic HI column density in the direction of the Lockman Hole (5.7×10^{19} cm^{-2}).

been observed (e.g., Comastri et al. 2001; Wilkes et al. 2002; Fiore et al. 2003; Brusa et al. 2003; Akiyama et al. 2003; Silverman et al. 2005; Gallagher et al. 2006; Hall et al. 2006; Tajer et al. 2007). Furthermore, all X-ray based classification schemes suffer from a serious redshift bias (as one observes higher redshift sources, the $2-10$ keV filter samples higher energies which are less affected by obscuring material, and the source appears softer; Szokoly et al. 2004). Figure 1.3, showing Γ_{eff} versus N_H for a range of redshifts, illustrates this effect – a higher redshift source with the same amount of obscuration has a higher value of Γ_{eff}.

The sources which show a discrepancy in their X-ray and optical indicators of absorption along the line-of-sight are not only problematic for mixed classification schemes, but also in terms of the validity of the simple unified model for AGNs (i.e., the homogeneous dust 'doughnut' surrounding the central engine). An important question is how many of the X-ray unabsorbed, optically obscured sources can be explained by the often invoked observational complications like host galaxy dilution (Moran et al. 2002; Severgnini et al. 2003; Hasinger et al. 2005), X-ray variability (Paolillo et al. 2004), and the redshifting of broad lines out of the spectral window (Silverman et al. 2005). If such sources cannot be explained as suffering from these observational complications, they lend support for the clumpy torus model (Risaliti et al. 2000; Hönig et al. 2006; Elitzur 2007; Nenkova et al. 2008) and torus-as-a-wind scenarios (Emmering et al. 1992; Konigl & Kartje 1994; Bottorff et al. 1997; Kartje et al. 1999). In the clumpy torus models, the probability for direct viewing of the central engine decreases away from the axis but is always finite (see Figure 1.4). These models also incorporate the change in cloud composition across the dust sublimation radius. While dusty material absorbs continuum radiation both in the UV/optical and X-ray, dust-free gas attenuates just the X-ray continuum. Clouds inside the dust sublimation radius therefore only provide obscuration in the X-ray regime. The combination of clumpiness and radius dependent dust-to-gas ratios allows for sources with differing X-ray and

optical spectral type.

A highly optically spectroscopically complete sample of X-ray selected AGNs will allow us to test the validity of the mixed classification scheme and reliably determine the percentage of AGNs whose X-ray properties indicate significant absorption but whose optical spectra show little obscuration, and vice-versa. We will be able to quantify how many sources with discrepant X-ray and optical properties can be explained by observational complications (like host galaxy dilution, X-ray variability, and the redshifting of broad lines), and whether a significant percentage truly do call for alterations to the simple unified model for AGNs.

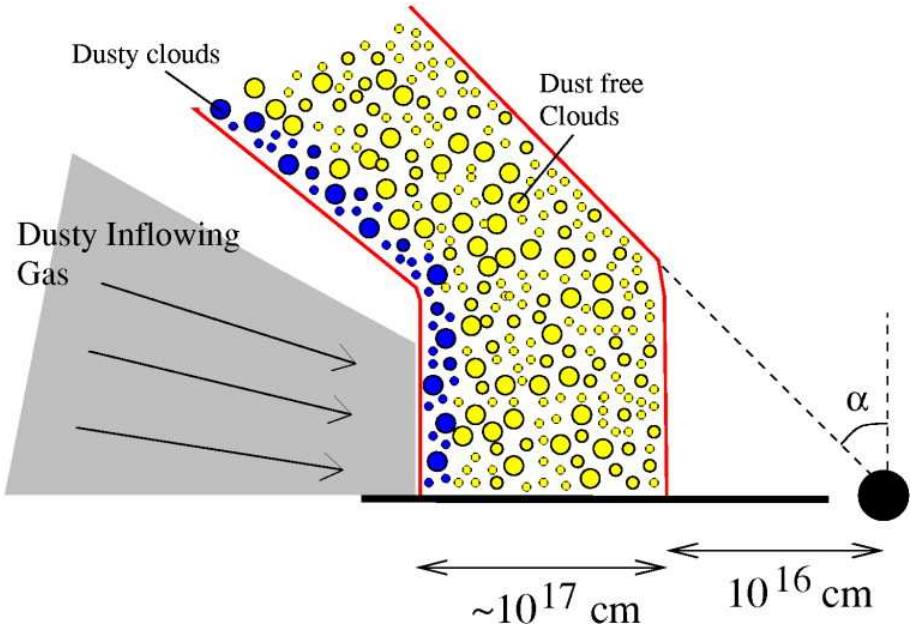

Fig. 1.4. — Clumpy torus model, derived from Elvis (2000) and further developed in Nenkova et al. (2008, and references therein). Reproduced from Risaliti et al. (2002).

1.3 Is [OIII] a Reliable Indicator of AGN Activity?

Kauffmann et al. (2003) and Heckman et al. (2004) proposed using the luminosity of the [OIII]λ5007Å (hereafter, [OIII]) line as a tracer of AGN activity, thus efficiently selecting AGNs from the large sample of galaxies in the Sloan Digital Sky Survey (SDSS). Narrow emission lines are thought to arise in gas excited by ionizing radiation escaping along the polar axis of the obscuring 'torus'. Since the narrow line region lies outside of the dusty circumnuclear material, the lines should not suffer from obscuration by that high column density material (though they may be affected by dust within the host galaxy). The [OIII] line is particularly appealing because it is one of the strongest narrow emission lines in optically obscured AGNs and the least contaminated by contributions from HII regions associated with star formation in the host galaxy (Heckman et al. 2005). While there is some evidence that the [OIII] luminosity is a good measure of AGN activity (e.g. Mulchaey et al. 1994), and, indeed, many researchers have assumed it to be so in their analyses (e.g. Alonso-Herrero et al. 1997; Hao et al. 2005; Netzer et al. 2006; Bongiorno et al. 2010), recent work has called this conclusion into question (e.g., Cocchia et al. 2007; Meléndez et al. 2008; Diamond-Stanic

et al. 2009; La Massa et al. 2009).

AGN activity can also be traced through the $2-10$ keV luminosity, although this measurement may suffer from some absorption (e.g., Diamond-Stanic et al. 2009; La Massa et al. 2009). Heckman et al. (2005) used their measurements of the ratio between X-ray and [OIII] luminosity to transform the Sazonov et al. (2004) *Rossi X-ray Timing Explorer (RXTE)* X-ray luminosity function (LF) into an [OIII] LF. They then compared this [OIII] LF with the SDSS [OIII] LF from Hao et al. (2005). They found that at the same equivalent luminosity, the space density of the hard X-ray selected AGNs was lower than that of the [OIII]-selected AGNs by a factor of ~ 0.5 dex. This led them to argue that selection by hard X-rays misses a significant fraction of the local AGN population with strong emission lines.

A large sample of X-ray selected AGNs with high optical spectroscopic completeness is ideal for investigating the reliability of the [OIII] emission line as an indicator of AGN activity. Such a sample can also test how many X-ray selected AGNs are misidentified as star formers by the commonly used Baldwin et al. (1981)-type narrow emission-line ratio empirical diagnostic diagram ([OIII]/Hβ versus [NII]/Hα, hereafter BPT diagram; see also Osterbrock et al. 1985 and Veilleux et al. 1987). Finally, redoing the Heckman et al. (2005) X-ray and [OIII] LF comparison with (1) a *Chandra* X-ray selected sample of AGNs combined with the *SWIFT BAT* results and (2) an updated understanding of the relation between the [OIII] and X-ray luminosities, will allow a more accurate estimate of the efficiency of optical versus X-ray selection of AGNs.

1.4 The Elusive Population of Compton-thick AGNs

The extragalactic XRB is thought to be mainly composed of the emission from accreting SMBHs throughout the history of the universe. The energy density of this cosmic radiation resides predominantly in the hard X-ray spectrum, which peaks at 30 keV. From the number density of known AGNs, we can estimate their contribution to the XRB. Optically bright quasars and Seyfert galaxies dominate at low energies (up to a few keV), while obscured AGNs, which outnumber unobscured ones by a factor of $3-4$ (Ueda et al. 2003; La Franca et al. 2005), are responsible for the bulk of the XRB at high energies ($>$ 10 keV). The ultradeep *Chandra* X-ray surveys have resolved nearly 100% of the $2-8$ keV XRB, but we appear to be missing up to 30% of the XRB at 30 keV (Gilli et al. 2007). The missing intensity of the XRB around 30 keV is attributed to the integrated emission from the elusive population of heavily X-ray absorbed, Compton-thick (CT) AGNs (with $N_H > 1.5 \times 10^{24}$ cm^{-2}). This missing population represents a significant fraction of the cosmic accretion onto SMBHs (Marconi et al. 2004).

This estimate for the number density of CT AGNs depends on (1) the true absolute intensity of the hard XRB, which is uncertain at the $10-30$% level, (2) the average broadband spectra of Compton-thin AGNs, and (3) the cosmological evolution of CT AGNs, which is assumed to be the same as Compton-thin AGNs.

After the first pioneering XRB measurements (Horstman et al. 1975), the *High Energy Astronomical Observatory* (*HEAO-1*) carried out a major effort in the late 1970s to obtain a reliable estimate of the XRB spectrum from $2-400$ keV (Marshall et al. 1980; Gruber et al. 1999). More recent experiments with the focusing telescopes aboard *BeppoSAX* (Vecchi et al. 1999), *XMM-Newton* (Lumb et al. 2002; De Luca & Molendi 2004), and *Chandra* (Hickox & Markevitch 2006) determined the $2-10$ keV XRB to be ~ 40%

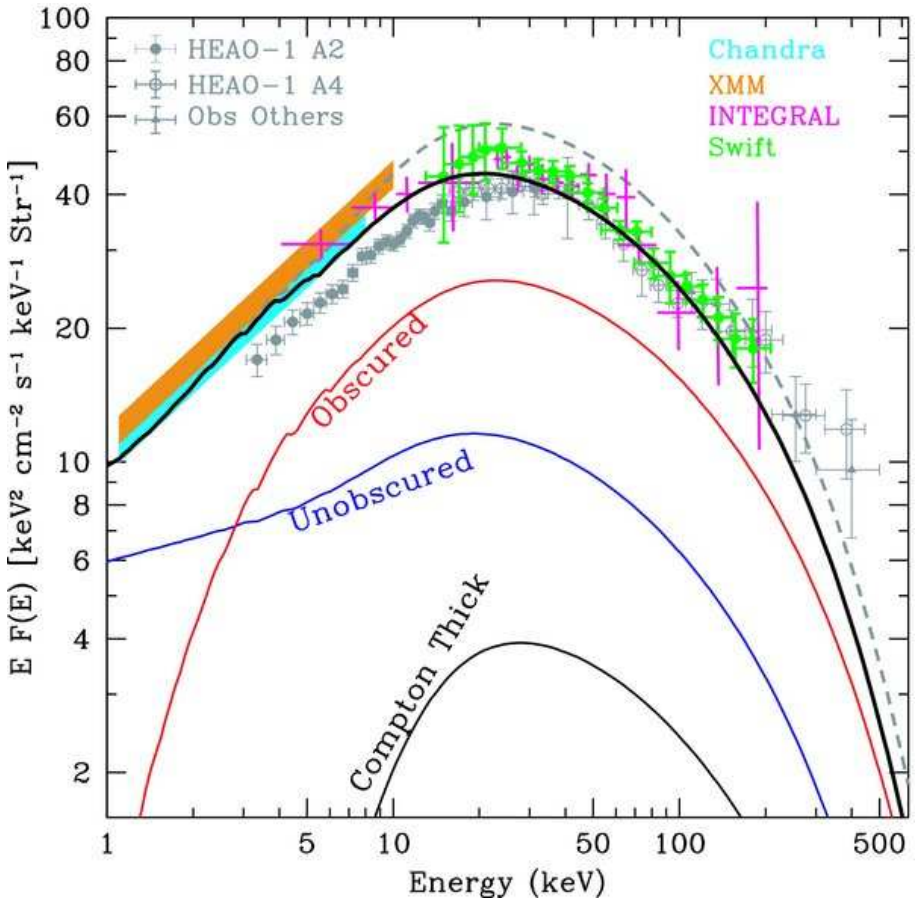

Fig. 1.5. — Observed spectrum of the extragalactic XRB from *HEAO-1* (Gruber et al. 1999), *Chandra* (Hickox & Markevitch 2006), *XMM-Newton* (De Luca & Molendi 2004), *INTEGRAL* (Churazov et al. 2007), and *Swift* (Ajello et al. 2008) data. The dashed gray line shows the XRB spectrum from the AGN population synthesis model of Treister et al. (2005), which assumed a 40% higher value for the *HEAO-1* XRB normalization. The thick black solid line shows the Treister et al. (2009) new population synthesis model for the XRB spectrum; the only change is the number of CT AGNs, which is reduced by a factor of 4 relative to the number in Treister et al. (2005). Reproduced from Treister et al. (2009).

higher than the *HEAO-1* estimate. Driven by these discordant results, several authors (Ueda et al. 2003; De Luca & Molendi 2004; Comastri 2004; Worsley et al. 2005; Worsley et al. 2006; Ballantyne et al. 2006; Hopkins et al. 2006), in their evaluation of the fraction of the XRB that can be resolved into individual sources, increased the *HEAO-1* XRB intensity by a factor of ~ 1.3 over the entire energy band (driving up the required number density of CT AGNs). Such a high value of the XRB intensity at $10 - 50$ keV is now ruled out by new *INTEGRAL* (Churazov et al. 2007), *Swift* (Ajello et al. 2008), and *BeppoSAX* (Frontera et al. 2007) data.

Treister et al. (2009) used these updated XRB measurements to create a new AGN population synthesis model with a more realistic prediction for the number density of CT AGNs. Figure 1.5 shows the results of this new population synthesis model (thick black line) compared to the measurements of the XRB by *HEAO-1*, *Chandra*, *XMM*, *INTEGRAL*, and *Swift*. The thin black line shows the predicted contribution to

the XRB from CT AGNs.

Assuming that the most recent XRB measurements are correct and that the new AGN population synthesis models are valid, one can then determine if there remains a significant population of missing sources by comparing the predicted number density of CT AGNs with the observed number density of CT AGNs.

The *Swift* and *INTEGRAL* ultra-hard X-ray detectors (> 15 keV) are sensitive to the direct emission from the central engine in transmission-dominated CT AGNs ($N_H \approx 10^{24} - 10^{25}$ cm^{-2}) and have helped constrain the observed number density of CT AGNs at very bright fluxes ($f_{17-70\mathrm{keV}} > 10^{-11}$ erg cm^{-2} s^{-1}) (Beckmann et al. 2006; Bassani et al. 2006; Sazonov et al. 2007; Winter et al. 2008; Winter et al. 2009; Tueller et al. 2010). These surveys, however, currently only probe out to $z < 0.05$ and miss the higher column density ($N_H > 10^{25}$ cm^{-2}), reflection-dominated CT AGNs.

Hard X-ray selection by *Chandra* or *XMM-Newton*, while being the most direct means currently to find obscured sources at high redshift, is limited by telescope sensitivities and wavelength coverage. Only the brightest sources with non-extreme column densities can be identified (Brandt & Hasinger 2005). For example, the archetype CT AGN NGC 1068, with $L_X = 10^{44}$ erg s^{-1}, would have a hard X-ray flux of only 7×10^{-18} erg cm^{-2} s^{-1} at $z = 2$, more than an order of magnitude fainter than that of sources detectable in the 2 Ms *Chandra* survey.

Some of the energy absorbed by the circumnuclear obscuring material is reprocessed and reemitted at longer wavelengths, allowing for detection in the infrared (IR). NGC 1068 would have a flux density of 25μJy at 24μm if placed at $z = 2$. While very faint, it would still be detectable in the ultradeep *Spitzer* MIPS (Rieke et al. 2004) image taken as part of the Great Observatories Origins Deep Survey (GOODS). The difficulty faced in mid-IR surveys is that the AGNs are vastly outnumbered by normal galaxies and some selection method is necessary to separate the two populations. Selection criteria which use *Spitzer*/IRAC mid-IR colors (Lacy et al. 2004; Stern et al. 2005) appear to be more prone to residual galaxy contamination at faint optical magnitudes or faint X-ray fluxes. Mid-IR spectral energy distribution (SED) techniques (Alonso-Herrero et al. 2006; Polletta et al. 2006; Donley et al. 2007) are more successful in picking out AGNs, but not necessarily the bulk of the CT AGN population.

Barger et al. (2007) used a highly spectroscopically complete deep VLA survey of the HDF-N region to examine whether radio sources can account for the missing $4 - 8$ keV light. They found that the X-ray faint and X-ray undetected radio sources contributed only a few percent of the light at these energies and cannot account for the background light missing at these energies.

Optical narrow emission lines offer an intriguing alternative route to identifying high-redshift CT AGNs. As discussed in the previous section, since the narrow line region lies outside of the dusty circumnuclear material, the lines should not suffer from obscuration by that high column density material. Optical emission line ratio diagnostics separate AGNs from star-forming galaxies. A highly optically spectroscopically complete sample of X-ray selected AGNs can be used to establish a reliable diagnostic that pushes to higher redshifts than the classic BPT diagram described in the previous section (which is limited to $z < 0.5$). With a highly optically spectroscopically complete sample of galaxies with overlying X-ray data, we can use these diagnostic diagrams to pick out AGNs and then, comparing their predicted, intrinsic X-ray luminosities with their observed X-ray luminosity, identify candidate CT AGNs. The number density of CT AGNs determined using optical emission lines will provide an essential complementary view of the high-redshift CT

AGN population to the mid-IR and radio selection.

1.5 The OPTX Survey Fields

While other X-ray surveys have numerous redshifts, they are relatively incomplete in heterogeneous ways (see Table 2.1). This thesis focuses on three of the most uniformly observed and spectroscopically complete surveys to date. The deep pencil-beam *Chandra* Deep Field-North (CDF-N) survey is the most spectroscopically complete of all of the X-ray survey fields. Our group (Barger et al. 2002; Barger et al. 2003; Barger et al. 2005; Trouille et al. 2008) has spectroscopically observed 91% of the sources in this field.

Our two intermediate-depth, wide-field surveys – the *Chandra* Lockman Area Synoptic Survey (CLASXS) and the *Chandra* Lockman Area North Survey (CLANS) – provide an essential step between the ultradeep narrow *Chandra* surveys and the shallow wide-area surveys. They cover large cosmological volumes, detect rare, high-luminosity AGNs, and robustly probe AGN evolution between $z \sim 0$ and 1. Our group (Steffen et al. 2004; Trouille et al. 2008; Trouille et al. 2009) has spectroscopically observed 89% of the sources in the CLASXS field and 76% of the sources in the CLANS field.

Overall, we have spectroscopically observed 96% of the OPTX sources above $f_{2-8\ \mathrm{keV}} = 10^{-14}$ erg s^{-1} cm^{-2} and 78% below, predominantly using the DEIMOS and HYDRA spectrographs.

1.5.1 CDF-N

The 2 Ms CDF-N survey, which covers the well-known *Hubble* Deep Field-North and flanking fields, is currently the deepest 'blank-field' X-ray survey (although the *Chandra* Deep Field-South has recently been allotted a total of 4 Ms). The CDF-N has revealed 503 X-ray sources over a ~ 460 arcmin^2 field-of-view to on-axis flux limits of 2.5×10^{-17} erg cm^{-2} s^{-1} and 1.4×10^{-16} erg cm^{-2} s^{-1} for the soft ($0.5 - 2$ keV) and hard ($2 - 8$ keV) X-ray bands, respectively (Alexander et al. 2003).

1.5.2 CLASXS & CLANS

The CLASXS and CLANS surveys sample large, contiguous solid angles (0.4 deg^2 and 0.6 deg^2, respectively) while remaining sensitive enough to measure $2 - 3$ times fainter than the observed break in the $2 - 8$ keV LogN-LogS distribution (Mushotzky et al. 2000). To minimize the effects of Galactic attenuation, CLASXS and CLANS are positioned in the Lockman Hole region of low HI galactic column density (Lockman et al. 1986).

The CLASXS survey consists of nine overlapping pointings with 40 ks exposures, except for the central pointing with 70 ks. This yields 525 X-ray sources with an on-axis $2 - 8$ keV flux limit of 6×10^{-15} erg cm^{-2} s^{-1}. The CLANS survey consists of nine slightly overlapping 70 ks pointings. This yields 761 X-ray sources with an on-axis $2 - 8$ keV flux limit of 3.5×10^{-15} erg cm^{-2} s^{-1}.

1.6 Thesis Goals and Outline

In this thesis I take advantage of the highly complete spectroscopic follow-up of the OPTX X-ray surveys to better understand the relation between the X-ray and optical spectral properties of AGNs. The

OPTX sample consists of 1789 sources in the CLANS, CLASXS, and CDF-N *Chandra* X-ray surveys covering 1.2 deg^2 of sky. The major goals of this thesis are to:

- Present the X-ray and optical photometric and spectroscopic data for the CLANS field and updated photometric and spectroscopic data for the CLASXS and CDF-N fields (Chapter 2).
- Compare the X-ray and optical spectral properties for a uniformly selected, highly spectroscopically complete sample of *Chandra* X-ray selected AGNs (Chapter 3).
- Determine the reliability of the [OIII] optical narrow emission line as an indicator of the ionizing flux from the central engine in AGNs (Chapter 4).
- Develop higher redshift optical narrow emission line ratio diagnostics that accurately identify X-ray selected AGNs (Chapter 5).
- Demonstrate that optical narrow emission line ratio diagnostics, when applied to galaxy samples with accompanying X-ray data, can be used to identify heavily X-ray absorbed, CT AGNs, providing an important alternative to mid-IR and radio searches (Chapter 5).

In Chapter 2 of this thesis I describe the creation of the X-ray catalog for the CLANS field and provide new (CLANS) and updated (CLASXS, CDF-N) redshift and optical/IR photometric catalogs for the three fields. In Chapter 3 I compare the optical spectral types with the X-ray spectral properties. In Chapter 4 I use the OPTX data to examine the reliability of optical emission line ratio diagnostics in identifying the distant X-ray AGN population and the reliability of the [OIII] emission line as an indicator of AGN activity. In Chapter 5 I use the OPTX sample to identify reliable high-redshift optical emission line ratio diagnostics. In applying these diagnostics to the highly optically spectroscopically complete sample of GOODS-N galaxies, I identify candidate CT AGNs and determine the number density for optically selected high-redshift CT AGNs. I give my conclusions, based on the results of my analyses, in Chapter 6.

This thesis encompasses all but one of the OPTX Project series articles (OPTX Project I, III, IV, and V). I have not included the analysis I carried out for the OPTX Project II article (Yencho et al. 2009). In this work, we combined the OPTX sample with the local *Swift* 9-month BAT sample to determine a local+distant hard X-ray luminosity function (HXLF) for the full sample and for the broad-line AGNs alone. We used a maximum likelihood method to find an analytic form for the HXLF, independent of the binning procedure, and presented the best-fit parameters for different luminosity and density dependent models.

References

Ajello, M., et al., 2008, ApJ, 689, 666

Akiyama, M., Ueda, Y., Ohta, K., Takahashi, T., & Yamada, T. 2003, ApJS, 148, 275

Alexander, D. M., et al., 2003, AJ, 126, 539

Alonso-Herrero, A., et al., 2006, ApJ, 640, 167

Alonso-Herrero, A., Ward, M. J., & Kotilainen, J. K. 1997, MNRAS, 288, 977

Antonucci, R. 1993, ARA&A, 31, 473

Baldwin, J. A., Phillips, M. M., & Terlevich, R. 1981, PASP, 93, 5

Ballantyne, D. R., Shi, Y., Rieke, G. H., Donley, J. L., Papovich, C., & Rigby, J. R. 2006, ApJ, 653, 1070

Barcons, X., Carrera, F. J., & Ceballos, M. T. 2003, MNRAS, 339, 757

Barden, S. C., Armandroff, T., Muller, G., Rudeen, A. C., Lewis, J., & Groves, L. 1994, in Proc. SPIE, Vol. 2198, 87–97

Barger, A. J., Cowie, L. L., Brandt, W. N., Capak, P., Garmire, G. P., Hornschemeier, A. E., Steffen, A. T., & Wehner, E. H. 2002, AJ, 124, 1839

Barger, A. J., et al., 2003, AJ, 126, 632

Barger, A. J., Cowie, L. L., Mushotzky, R. F., Yang, Y., Wang, W.-H., Steffen, A. T., & Capak, P. 2005, AJ, 129, 578

Barger, A. J., Cowie, L. L., & Wang, W. 2007, ApJ, 654, 764

Bassani, L., et al., 2006, ApJ, 636, L65

Beckmann, V., Soldi, S., Shrader, C. R., Gehrels, N., & Produit, N. 2006, ApJ, 652, 126

Bongiorno, A., et al. 2010, A&A, 510, A56

Bottorff, M., Korista, K. T., Shlosman, I., & Blandford, R. D. 1997, ApJ, 479, 200

Brandt, W. N., et al., 2001, AJ, 122, 2810

Brandt, W. N. & Hasinger, G. 2005, ARA&A, 43, 827

Brusa, M., et al., 2003, A&A, 409, 65

Caccianiga, A., et al., 2004, A&A, 416, 901

Cardamone, C. N., Moran, E. C., & Kay, L. E. 2007, AJ, 134, 1263

Churazov, E., et al., 2007, A&A, 467, 529

Cocchia, F., et al., 2007, A&A, 466, 31

Comastri, A. 2004, in Supermassive Black Holes in the Distant Universe, ed. A. J. Barger, Vol. 308, 245

Comastri, A., Fiore, F., Vignali, C., Matt, G., Perola, G. C., & La Franca, F. 2001, MNRAS, 327, 781

Corral, A., Barcons, X., Carrera, F. J., Ceballos, M. T., & Mateos, S. 2005, A&A, 431, 97

Cowie, L. L., Barger, A. J., & Trouille, L. 2009, ApJ, 692, 1476

De Luca, A. & Molendi, S. 2004, A&A, 419, 837

Diamond-Stanic, A. M., Rieke, G. H., & Rigby, J. R. 2009, ApJ, 698, 623

Donley, J. L., Rieke, G. H., Pérez-González, P. G., Rigby, J. R., & Alonso-Herrero, A. 2007, ApJ, 660, 167

Elitzur, M. 2007, in ASPC, Vol. 373, The Central Engine of Active Galactic Nuclei, ed. L. C. Ho & J.-W. Wang, 415

Elvis, M. 2000, ApJ, 545, 63

Elvis, M., Risaliti, G., Nicastro, F., Miller, J. M., Fiore, F., & Puccetti, S. 2004, ApJ, 615, L25

Emmering, R. T., Blandford, R. D., & Shlosman, I. 1992, ApJ, 385, 460

Faber, S. M., et al., 2003, Proc. SPIE, 4841, 1657

Ferrarese, L. & Merritt, D. 2000, ApJ, 539, L9

Fiore, F., et al., 2003, A&A, 409, 79

Frontera, F., et al., 2007, ApJ, 666, 86

Gallagher, S. C., Brandt, W. N., Chartas, G., Priddey, R., Garmire, G. P., & Sambruna, R. M. 2006, ApJ, 644, 709

Garcet, O., et al., 2007, A&A, 474, 473

Gebhardt, K., et al., 2000, ApJ, 539, L13

Georgantopoulos, I. & Zezas, A. 2003, ApJ, 594, 704

Giacconi, R. et al. 2002, ApJS, 139, 369

Gilli, R., Comastri, A., & Hasinger, G. 2007, A&A, 463, 79

Gruber, D. E., Matteson, J. L., Peterson, L. E., & Jung, G. V. 1999, ApJ, 520, 124

Hall, P. B., Gallagher, S. C., Richards, G. T., Alexander, D. M., Anderson, S. F., Bauer, F., Brandt, W. N., & Schneider, D. P. 2006, AJ, 132, 1977

Hao, L., et al., 2005, AJ, 129, 1795

Hasinger, G., Miyaji, T., & Schmidt, M. 2005, A&A, 441, 417

Heckman, T. M., Kauffmann, G., Brinchmann, J., Charlot, S., Tremonti, C., & White, S. D. M. 2004, ApJ, 613, 109

Heckman, T. M., Ptak, A., Hornschemeier, A., & Kauffmann, G. 2005, ApJ, 634, 161

Hickox, R. C. & Markevitch, M. 2006, ApJ, 645, 95

Hönig, S. F., Beckert, T., Ohnaka, K., & Weigelt, G. 2006, A&A, 452, 459

Hopkins, P. F., Hernquist, L., Cox, T. J., Di Matteo, T., Robertson, B., & Springel, V. 2006, ApJS, 163, 1

Horstman, H. M., Cavallo, G., & Moretti-Horstman, E. 1975, Nuovo Cimento Rivista Serie, 5, 255

Kartje, J. F., Königl, A., & Elitzur, M. 1999, ApJ, 513, 180

Kauffmann, G., et al., 2003, MNRAS, 346, 1055

Konigl, A. & Kartje, J. F. 1994, ApJ, 434, 446

Kormendy, J. & Richstone, D. 1995, ARA&A, 33, 581

La Franca, F., et al., 2005, ApJ, 635, 864

La Massa, S. M., Heckman, T. M., Ptak, A., Hornschemeier, A., Martins, L., Sonnentrucker, P., & Tremonti, C. 2009, ApJ, 705, 568

Lacy, M., et al., 2004, ApJS, 154, 166

Lockman, F. J., Jahoda, K., & McCammon, D. 1986, ApJ, 302, 432

Lumb, D. H., Warwick, R. S., Page, M., & De Luca, A. 2002, A&A, 389, 93

Luo, B. et al. 2008, ApJS, 179, 19

Magorrian, J., et al., 1998, AJ, 115, 2285

Marconi, A., Risaliti, G., Gilli, R., Hunt, L. K., Maiolino, R., & Salvati, M. 2004, MNRAS, 351, 169

Marshall, F. E., Boldt, E. A., Holt, S. S., Miller, R. B., Mushotzky, R. F., Rose, L. A., Rothschild, R. E., & Serlemitsos, P. J. 1980, ApJ, 235, 4

Mateos, S., Barcons, X., Carrera, F. J., Ceballos, M. T., Hasinger, G., Lehmann, I., Fabian, A. C., & Streblyanska, A. 2005, A&A, 444, 79

Meléndez, M., et al., 2008, ApJ, 682, 94

Moran, E. C., Filippenko, A. V., & Chornock, R. 2002, ApJ, 579, L71

Mulchaey, J. S., Koratkar, A., Ward, M. J., Wilson, A. S., Whittle, M., Antonucci, R. R. J., Kinney, A. L., & Hurt, T. 1994, ApJ, 436, 586

Mushotzky, R. F., Cowie, L. L., Barger, A. J., & Arnaud, K. A. 2000, Nature, 404, 459

Mushotzky, R. F. 2004, in Supermassive Black Holes in the Distant Universe, ed. A. J. Barger, Vol. 308, 53

Nenkova, M., Sirocky, M. M., Nikutta, R., Ivezic, I., & Elitzur, M. 2008, ApJ

Netzer, H., Mainieri, V., Rosati, P., & Trakhtenbrot, B. 2006, A&A, 453, 525

Osterbrock, D. E. & Pogge, R. W. 1985, ApJ, 297, 166

Panessa, F. & Bassani, L. 2002, A&A, 394, 435

Paolillo, M., Schreier, E. J., Giacconi, R., Koekemoer, A. M., & Grogin, N. A. 2004, ApJ, 611, 93

Pappa, A., Georgantopoulos, I., Stewart, G. C., & Zezas, A. L. 2001, MNRAS, 326, 995

Polletta, M. d. C., et al., 2006, ApJ, 642, 673

Rieke, G. H. et al. 2004, ApJS, 154, 25

Risaliti, G., Elvis, M., Fabbiano, G., Baldi, A., & Zezas, A. 2005, ApJ, 623, L93

Risaliti, G., Elvis, M., Fabbiano, G., Baldi, A., Zezas, A., & Salvati, M. 2007, ApJ, 659, L111

Risaliti, G., Elvis, M., & Nicastro, F. 2002, ApJ, 571, 234

Risaliti, G., Maiolino, R., & Bassani, L. 2000, A&A, 356, 33

Sazonov, S., Revnivtsev, M., Krivonos, R., Churazov, E., & Sunyaev, R. 2007, A&A, 462, 57

Sazonov, S. Y. & Revnivtsev, M. G. 2004, A&A, 423, 469

Severgnini, P., et al., 2003, A&A, 406, 483

Silverman, J. D., et al., 2005, ApJ, 618, 123

Steffen, A. T., Barger, A. J., Capak, P., Cowie, L. L., Mushotzky, R. F., & Yang, Y. 2004, AJ, 128, 1483

Stern, D., et al. , 2005, ApJ, 631, 163

Szokoly, G. P., et al., 2004, ApJS, 155, 271

Tajer, M., et al., 2007, A&A, 467, 73

Tozzi, P., et al., 2006, A&A, 451, 457

Treister, E. & Urry, C. M. 2005, ApJ, 630, 115

Treister, E., Urry, C. M., & Virani, S. 2009, ApJ, 696, 110

Trouille, L., Barger, A. J., Cowie, L. L., Yang, Y., & Mushotzky, R. F. 2008, ApJS, 179, 1

—. 2009, ApJ, 703, 2160

Tueller, J., et al., 2010, ApJS, 186, 378

Ueda, Y., Akiyama, M., Ohta, K., & Miyaji, T. 2003, ApJ, 598, 886

Urry, C. M. & Padovani, P. 1995, PASP, 107, 803

van der Marel, R. P. 1999, AJ, 117, 744

Vecchi, A., Molendi, S., Guainazzi, M., Fiore, F., & Parmar, A. N. 1999, A&A, 349, L73

Veilleux, S. & Osterbrock, D. E. 1987, ApJS, 63, 295

Wilkes, B. J., Schmidt, G. D., Cutri, R. M., Ghosh, H., Hines, D. C., Nelson, B., & Smith, P. S. 2002, ApJ, 564, L65

Winter, L. M., Mushotzky, R. F., Reynolds, C. S., & Tueller, J. 2009, ApJ, 690, 1322

Winter, L. M., Mushotzky, R. F., Tueller, J., & Markwardt, C. 2008, ApJ, 674, 686

Wolter, A., Gioia, I. M., Henry, J. P., & Mullis, C. R. 2005, A&A, 444, 165

Worsley, M. A., Fabian, A. C., Bauer, F. E., Alexander, D. M., Brandt, W. N., & Lehmer, B. D. 2006, MNRAS, 368, 1735

Worsley, M. A., et al., 2005, MNRAS, 357, 1281

Yencho, B., Barger, A. J., Trouille, L., & Winter, L. M. 2009, ApJ, 698, 396